Estimation of precipitation over Asia by combined use of gauge and multi-satellite sensor observations at fine scale

Anoop Mishra[1], A. Yatagai[1], A. Hamada[1], and R. M. Gairola[2]

[1]Research Institute for Humanity and Nature, Kyoto, Japan

[2] Space Applications Centre, ISRO, Ahmedabad, India

In the present study an effort is made to estimate 3-hourly rainfall using gauge and satellite observations over land and oceanic region of Asia (40°S-50°N, 40°E-130°E) at 0.25° ×0.25° spatial resolution. The study utilizes observations from rain gauge, Special Sensor Microwave/Imager (SSM/I) onboard Defense Meteorological Satellite Program (DMSP), Precipitation Radar (PR) onboard Tropical Rainfall Measuring Mission (TRMM) and geo-stationary satellite Meteosat from Eumetsat. The present study makes use of rainfall estimates by synergistic use of multi-satellite sensors using Meteosat Infrared and Water Vapor absorption channel and PR observations (Mishra et al., 2009, 2010) and SSM/I derived microwave estimates using regional scattering index developed by Mishra et al. (2009). Over orographic region a new relationship is developed using meteosat and rain-gauge observations between rainfall and brightness temperature. The rain areas over the land portion of area of study is filled by available rain gauge observations but if the rain gauge observations are unavailable the vacant area is filled by available microwave observations followed by the microwave calibrated infrared observations over the land and oceanic region of area of study. The precipitation estimates from the present approach is validated against rain gauge observations and other available standard rainfall products. The validation results show that present approach of precipitation estimation is able to estimate the rainfall with a very good accuracy.

1. Introduction

Rainfall is one of the most unusually discontinuous atmospheric phenomena owing to its high spatial and temporal variability. The accurate forecasting of rainfall is important to agriculture. Furthermore, an accurate assessment of rainfall is required to analyze the total water budget of earth–atmosphere systems. The main source of rainfall over South Asia is the monsoon; therefore, a robust rainfall algorithm for the pre-monsoon, monsoon, and post-monsoon periods is required.

Over South Asia and adjoining oceans, reliable data are provided by ground-based radar and a dense network of rain gauges in limited areas. For synoptic applications, satellite-based estimates are highly desired. Standard estimations based on satellite infrared (IR) measurements have high temporal resolution. However, these estimates have large errors because IR radiance from cloud tops has only an indirect and weak relationship with surface rainfall. The most common rainfall-estimation technique of using the Geostationary

Operational Environment Satellite (GOES) precipitation index (Arkin and Meisner, 1987), based on a simple infrared-brightness temperature (IR-TB) threshold algorithm, has been employed to produce tropical and subtropical precipitation products on large temporal and spatial scales for use in climatological studies.

Although satellite microwave (MW) measurements have good physical connection with rain and hydrometeors but are at a disadvantage on temporal and spatial scale because of coarser spatial resolution, and lower orbiting satellites provide less coverage. The development of hybrid techniques using the strengths of MW and IR radiation, based on proper intercalibration over common areas, is therefore highly desirable. Adler et al. (1994) noted that there are opportunities to improve precipitation estimates by combining two types of data so that the strengths of individual techniques are maintained and the weaknesses are compensated for. Over the last few years, a number of groups have embarked on the development of so-called hybrid techniques through synergistic use of multi-satellite sensor observations (Jobard and Desbois, 1994; Mishra et al., 2009, 2010).

The present study estimates rainfall over South Asia by combining rain gauge and merged satellite observations. The present rainfall estimates are validated using Automatic Weather Station (AWS) rain gauge data and other available rainfall products such as those of Asian Precipitation—Highly Resolved Observational Data Integration Towards Evaluation (APHRODITE) and TRMM-3B42.

2. Data sources

The primary data used in this study are (1) IR and water vapor (WV) observations made by geostationary satellites and (2) MW observations made by Tropical Rainfall Measuring Mission (TRMM) and Defense Meteorological Satellite Program (DMSP) satellites, which are in low Earth orbits. Conventional data were obtained from the AWS network for validation. The estimates were intercompared using available standard products such as APHRODITE, and TRMM-3B42V6.

2.1. Meteosat and TRMM satellite data

Meteosat is a geostationary Earth-observation satellite launched by the European Space Agency and now operated by the European Organization for the exploitation of Meteorological Satellites. It provides thermal infrared (TIR) and WV images at half-hourly intervals with spatial resolution of 4 km. In the present study, we use TIR and WV data from Meteosat-7.

The TRMM, launched in late November 1997 into a near-circular orbit with 35° inclination from the equatorial plane, provides data recorded by passive instruments in the optical and MW regions. It also carries a Precipitation Radar (PR). We use the surface rainfall data of Precipitation Radar Version 6 (2A25) (Iguchi et al., 2000) and Meteosat IR and WV data for development of the algorithm, and a standard merged IR and MW data product called 3B42 (Huffman et al., 2007) for the intercomparison.

2.2. AWS rain gauge data

The AWS designed by the Indian Space Research Organization (ISRO) is a compact, modular, rugged, powerful and low-cost system housed in a portable, self-contained package. In contrast to many other sensors, it has a tipping bucket rain gauge with unlimited rain measuring capacity and accuracy better than 1 mm. The data are relayed through a satellite and made available on the website www.mosdac.gov.in. For development and validation of the present algorithm, AWS rain gauge data for 2007, 2008, 2009, and 2010 are used. The AWS distribution over India is shown in Figure 1.

2.3. APHRODITE (V1003) data

For qualitative and quantitative comparison of the rainfall derived employing the present technique, we use the APHRODITE product V1003 (Yatagai et al., 2009), which was developed for the period from 1951 to 2007 over monsoon Asia in 0.25° × 0.25° grid cells from observations made by a dense network of rain gauges.

2.4. Special Sensor Microwave/Imager (SSM/I) data

The SSM/I instrument was developed as part of the DMSP and was flown aboard the Air Force Block 5D polar-orbiting satellite on June 19, 1987. The sensor built by Hughes Aircraft Company operates at four frequencies of 19.35, 22.235, 37.0, and 85.5 GHz. All frequencies except the WV absorption channel at 22.235 GHz are dual polarized. The resolution depends on the frequency and ranges from approximately 50 km at 19 GHz to 15 km at 85.5 GHz. The present study takes SSM/I (F13) data for the years 2007, 2008, 2009, and 2010.

3. Methodology

In the present study, rainfall over the study area is estimated by combining rain gauge and satellite observations. The southern part of the study area (around 14°N and 78°E) has a dense network of ISRO AWS rain gauges (shown by the bounded box in Figure 1). The density of gauges is such that at least two to six gauges fall within a 0.25° × 0.25° cell over most of the region. Spatially averaged rainfall estimates were made using a simple spatial averaging technique. If there were fewer than two gauges in a 0.25° × 0.25° cell, then the pixels within the cell were calibrated through weighted averaging making use of the Meteosat IR-TB data by matching the rainfall recorded by rain gauges with the Meteosat brightness temperature.

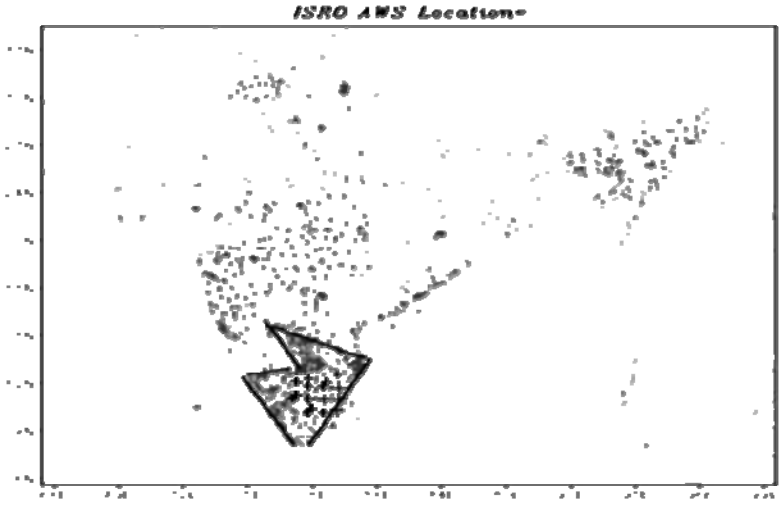

Fig. 1. ISRO AWS rain gauge distribution over the study area. Stations for which data are used in developing the algorithm are shown by the black bounded box.

The rainfall over the southern land area was estimated from rain gauge observations. Rainfall over the remaining study area was estimated from SSM/I observations employing a regional scattering index technique (Mishra et al., 2009) developed separately for land and ocean in the study area.

The procedure consists of two steps. In the first step, a region-specific 'scattering index' is developed by combining the signals of the 19, 22 and 85 GHz channels, treating the land and oceanic regions separately. The second step establishes a new relationship between the scattering index and the rain rate using TRMM PR data, mainly following Ferraro and Marks (1995).

To develop the scattering index, a relationship for 19, 22 and 85 GHz channels is established under non-rainy conditions:

$$F=A+B\times Tv(19)+C\times Tv(22)+D\times (Tv(22))^2 \quad (1)$$

where F is the brightness temperature of the 85 GHz channel and Tv(f) is the vertically polarized brightness temperature at frequency f. For land regions, the coefficients are A = 448.6809, B = –1.5456, C = –0.6020, and D = 0.0055. For oceanic regions, the coefficients are A = –362.4467, B = 1.1379, C = 3.5247, and D = –0.0078. After A, B, C and D are calculated, F is obtained, and the scattering index for the 85 GHz channel is defined as

$$SI(85) = F - Tv(85) \quad (2)$$

for the entire database (both raining and non-raining signals). From this step onwards, the index SI is used to separate the scattering and non-scattering signals for a given set of independent data. The SI was calibrated with PR measurements. Using separate relations for the land and ocean (Figures 2a and 2b) has been found to work best (Mishra et al., 2009).

For land,

$$RR\ (m/h) = .0268\times (SI)^{1.5978} \quad (3)$$

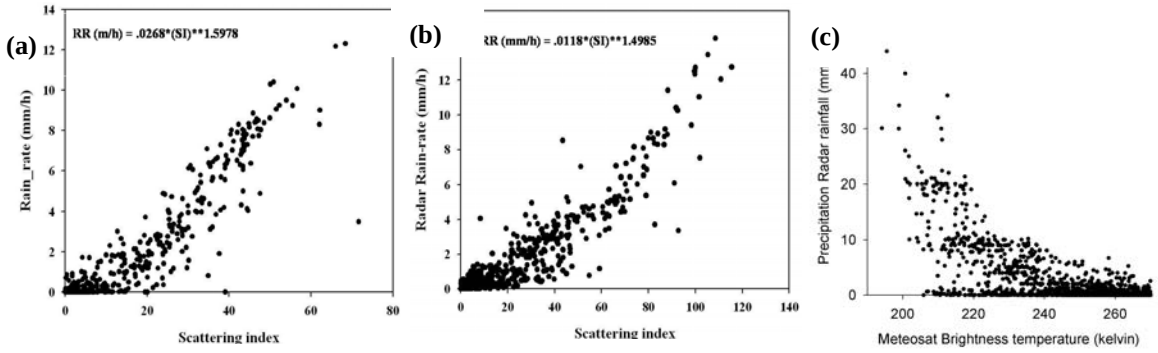

Fig. 2. Relationship between the scattering index derived from the SSM/I and rainfall derived from the PR for (a) land and (b) ocean. (c) Relationship between the Meteosat brightness temperature and PR rain rates.

and for ocean,

$$RR\ (mm/h) = .0118 \times (SI)^{1.4985} \quad (4)$$

where RR is the rain rate in millimeters per hour.

The above two equations for land and ocean were applied to obtain the rainfall using the scattering index derived from SSM/I observations.

If rain gauge and MW observations were missing, then (temporal and spatial) gaps over the study area were filled with MW-calibrated IR observations through the synergistic use of multi-satellite sensor observations (Mishra et al., 2010).

The procedure begins with a cloud classification scheme following Roca et al. (2002) and using Meteosat IR and WV channels to identify thin cirrus, deep convective and very deep convective clouds over 0.25° × 0.25° grid cells. Subsequently, IR-TB values were calibrated (Figure 2c) using PR rainfall within 15 minutes of difference, for which the autocovariance function of rainfall reduces to approximately 0.9. Since TIR and PR measurements have nearly identical spatial resolution (4–5 km), non-uniformity was not considered on a finer scale. Finally, the rainfall rate was calculated using a nonlinear power law relation between the collocated and near-simultaneous IR-TB and PR rainfall rate in a 0.25° × 0.25° cell. Applying both linear and nonlinear regression between the IR-TB and rainfall rate, it was found that the following power-law regression equation best explains the relationship between the two variables (Mishra et al., 2010):

$$RR = 16.6614 \times \exp(-(TB - 204.57)/16.52688) \quad (5)$$

Therefore, the rainfall in areas for which there were no rain gauge and MW observations was estimated by applying the above equation to Meteosat data.

4. Results and discussions

The present technique was developed by merging rain gauge, MW and MW-calibrated IR observations. Employing this technique, rainfall datasets for the years 2007, 2008, 2009, and 2010 were created.

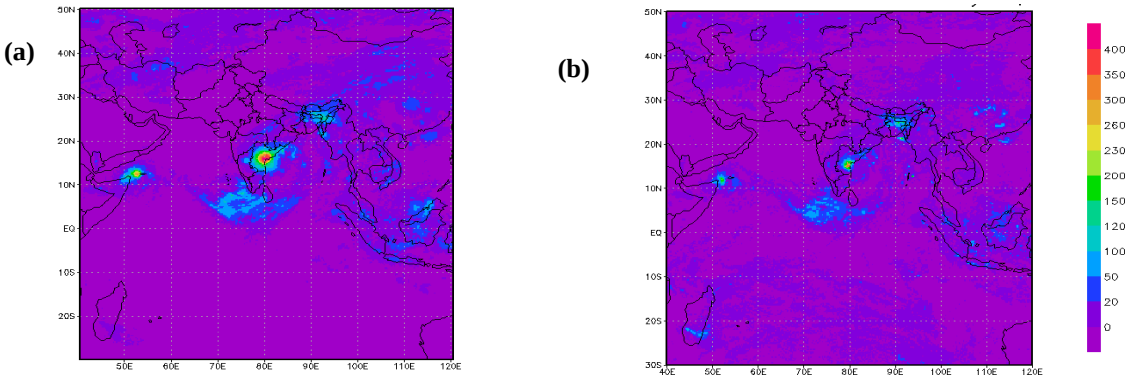

Fig. 3. Twenty-four-hour accumulated rainfall on 20 May 2010 in 0.25° × 0.25° cells derived (a) using the present technique and (b) from TRMM-3B42V6.

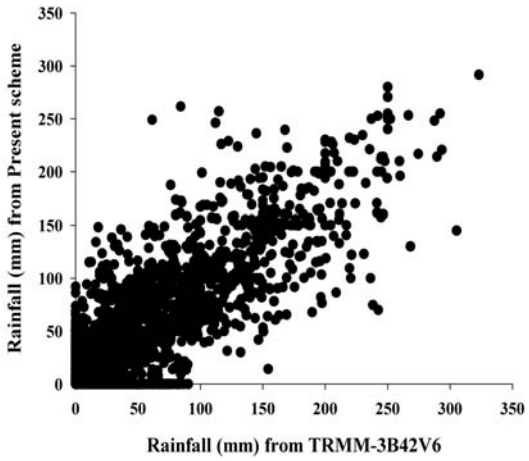

Fig. 4. Scatterplot of daily rainfall in 0.25° × 0.25° cells derived from TRMM-3B42V6 and employing the present scheme.

Table 1.

No. Of data points	**61064**
Correlation coefficients	**0.86**
Root Mean Square Error (mm)	**15.28**
Bias (mm)	**1.12**
TRMM-3B42 mean (mm)	**10.68**
Present scheme mean (mm)	**11.80**
Probability of detection (POD)	**0.72**
False Alarm Ratio (FAR)	**0.25**
Heidke Skill Score	**0.23**

The usefulness of the technique was examined by applying it to a recent cyclonic event. Only one case study is presented for brevity.

To compare the daily accumulated rainfall in 0.25° × 0.25° cells over the study area derived employing the present scheme with that derived from TRMM-3B42V6, we selected the case of the recent tropical cyclone Laila, which developed on 17 May 2010 over the Bay of Bengal. Figures 3a and 3b present the rainfall associated with the landfall of tropical cyclone Laila over the Andhra Pradesh coast on 20 May 2010 as derived using the present technique and derived from TRMM-3B42 respectively. The figures confirm that the present scheme reasonably depicts the pattern and intensity of rain in that they consistently match the pattern and intensity derived from TRMM-3B42V6 observations. Furthermore, for the quantitative

assessment of the present scheme, 61,064 temporally and spatially collocated data points of daily accumulated rainfall for the periods 1–5 July, 11–19 August, and 12–14 December 2008, 12–17 September and 24–26 November 2009, and 17–21 May and 25– 28 June 2010 derived using the present technique and derived from TRMM-3B42V6 over the study area in 0.25° × 0.25° cells were considered. Figure 4 is a scatterplot of the two rainfall estimates, and Table 1 presents the associated statistics. Rainfall derived using the present technique and that derived from TRMM-3B42 V6 have a correlation coefficient of 0.86, root-mean-square error of 15.28, bias of 1.12, probability of detection of 0.72, false alarm ratio of 0.25, and skill score of 0.23. In Figure 4, we note a reasonable number of high rainfall points for the present scheme that are underestimated by the TRMM-3B42V6 observations. This may be due to TRMM-3B42V6 tending to underestimate orographic rain (Rahman et al., 2009), which may be depicted well by the present technique.

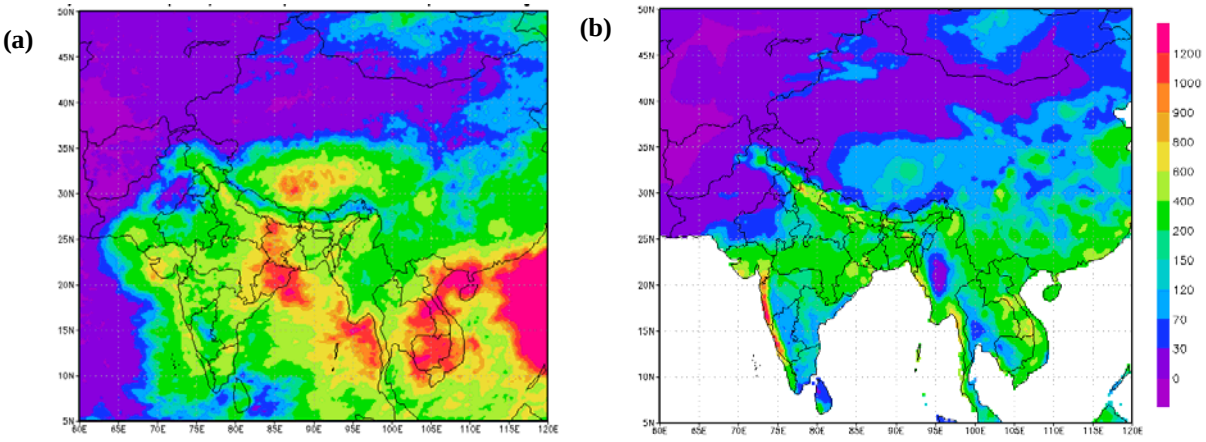

Fig. 5. Monthly accumulated rainfall (mm) over 0.25° × 0.25° grid box during August 2007 (a) from present technique (b) from the APHRODITE product.

To further evaluate the performance of the present scheme, we compared its rainfall results with the rain-gauge-based product APHRODITE (V1003). Figures 5a and 5b show the monthly rainfall during August 2007 derived using the present technique and that derived from APHRODITE (V1003) observations, respectively. The figures clearly show that during this period, the monsoon covered the whole Indian region, bringing heavy rainfall to the southern and western Indian coasts and central and northeastern India. The Tibetan Plateau also experienced spells of heavy rainfall (Figure 5a). Rainfall derived using present technique and that from the APHRODITE observations matches qualitatively with few exceptions. Rainfall over the central and northern India is in the same range from both observations.

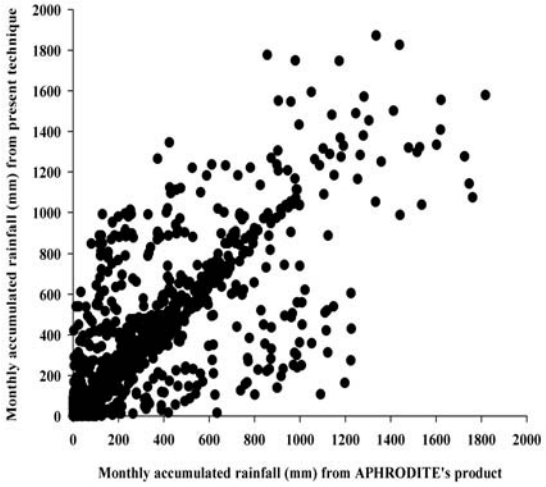

Fig. 6. Scatterplot of monthly rainfall in 0.25° × 0.25° cells derived from APHRODITE data and using the present scheme.

Table 2.

No. Of data points	**12645**
Correlation coefficients	**0.68**
Root Mean Square Error (mm)	**172.56**
Bias (mm)	**23.75**
APHRODITE's mean (mm)	**179.86**
Present scheme mean (mm)	**203.61**
Probability of detection (POD)	**0.71**
False Alarm Ratio (FAR)	**0.37**
Heidke Skill Score	**0.24**

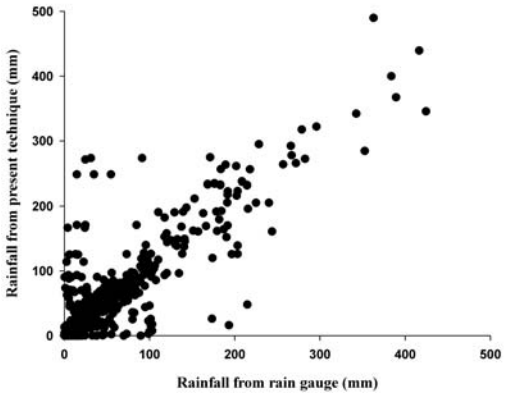

Fig. 7. Scatterplot of rainfall in 0.25° × 0.25° cells derived using the present scheme and rain gauge observations.

Table.3

No. Of data points	**1371**
Correlation coefficients	**0.77**
Root Mean Square Error (mm)	**27.14**
Bias (mm)	**2.71**
Rain gauge mean (mm)	**24.06**
Present scheme mean (mm)	**26.77**
Probability of detection (POD)	**0.83**
False Alarm Ratio (FAR)	**0.34**
Heidke Skill Score	**0.29**

APHRODITE observations give higher levels of rainfall over the southern and western coasts than the present technique, while rainfall over the Tibetan Plateau is greater when employing the present technique.

Figure 6 is a scatterplot of rainfall derived from the present technique and that derived from APHRODITE observations over 5°N–50°N and 60°E–120°E in 0.25° × 0.25° cells, and Table 2 gives the associated statistics. For this purpose, 12,645 data points for January, July, and September 2007 were considered. Rainfall derived using the present technique and that derived from APHRODITE observations have a correlation coefficient of 0.68, root-mean-square error

of 172.56, bias of 23.75, probability of detection of 0.71, false alarm ratio of 0.37, and a skill score of 0.24. From the statistics, it is clear that the present technique retrieves rainfall values that are quite consistent with those derived from APHRODITE observations with few exceptions.

Finally, the daily accumulated rainfall derived using the present scheme is validated against rain gauge observations over land in India in 0.25° × 0.25° cells. For this purpose, 1371 spatially and temporally collocated data points obtained using the present scheme and derived from rain gauge observations for the periods 17–25 June and 12–17 September 2007, 16–21 July, 7–11 August and 19–21 November 2008, and 1–5 March and 18–24 May 2009 were considered. Figure 7 is a scatterplot and Table 3 gives the associated statistics. The two estimates in Fig. 7 have a correlation coefficient of 0.77, root-mean-square error of 27.14 mm/day, bias of 2.71 mm/day, probability of detection of 0.83, false alarm ratio of 0.34, and a skill score of 0.29.

5. Summary and conclusions

The present study describes the development of a (daily accumulated) rainfall product for the period 2007–2010 over South Asia (30°S–50°N, 40°E–120°E) at 0.25° × 0.25° spatial resolution. The rain rates are derived by merging rain gauge and multi-sensor satellite observations. Validation and statistical analysis were performed using ground observations and other satellite rainfall products. Validation with the rain gauges and comparison with other rainfall products shows that the present approach of rainfall estimation estimates the rainfall over South Asia with good accuracy. There are several rainfall products available for research purposes; e.g., the rain-gauge-based APHRODITE water resources over Asia product (Yatagai et al., 2009) and global rainfall products such as TRMM-3B42 V6, GPCPV2, Climate Prediction Centre Morphing (CMORPH) (Joyce et al., 2004), and Global Satellite Mapping of Precipitation (GSMaP) products (Kubota et al., 2007). The rain-gauge-based product does not provide information on oceanic regions, while the other global rainfall products mentioned above rely on rainfall estimation based on proxy variables such as the polarization-corrected temperature (Spencer et al., 1989) and scattering indices (Ferraro and Marks, 1995), which vary with region and season and do not perform well for South Asia (Mishra et al., 2009). The present rainfall product based on rain gauge and MW observations using a regional scattering index and region-specific MW-calibrated infrared observations developed for South Asia gives good estimates of the rainfall over land and ocean in South Asia for research purposes.

Acknowledgement

This research was supported by the Environment Research and Technology Development Fund (A-0601) of the Ministry of the Environment, Japan. We thank the Ministry of the Environment, Japan, for a fund awarded through the E. F. Fellowship (A06018). We appreciate TRMM-3B42V6, APHRODITE, SSM/I, AWS, and Meteosat data being made available.

References

1. Adler, R.F, G.J Huffman and P.R. Keehn (1994), Global rain estimates from microwave adjusted geosynchronous IR data, Remote Sensing Review, 11, pp.125-135.
2. Adler, R.F., G.J. Huffman, A. Chang, R. Ferraro, P. Xie, J. Janowiak, B. Rudolf, U. Schneider, S. Curtis, D. Bolvin, A. Gruber, J. Susskind, P. Arkin, and E., Nelkin (2003), The Version 2 Global Precipitation Climatology Project (GPCP) Monthly Precipitation Analysis (1979-Present). Journal of Hydrometeorology, 4, pp.1147-1167.
3. Arkin P.A., and B.N. Meisner (1987), The relationship between large scale convective rainfall and cold cloud cover over the Western Hemisphere during 1982-1984, Monthly Weather Review, 115, pp. 51-74.
4. Ferraro, R.R. and G.F. Marks (1995), The development of SSM/I rain rate retrieval algorithms using ground based radar measurements, Journal of Atmospheric and Oceanic Technology, 12, pp. 755-770.
5. Huffman, G. J., R. F. Adler, D. T. Bolvin, G. Gu, E. J. Nelkin, K. P. Bowman, Y. Hong, E. F. Stocker, and D. B. Wolf (2007), The TRMM Multisatellite Precipitation Analysis (TMPA): Quasi-Global, Multiyear, Combined-Sensor Precipitation Estimates at Fine Scales, Journal of Hydrometeorology, 8, pp. 38-55.
6. Iguchi T, T. Kozu, R. Meneghini, J. Awaka and K. Okamoto (2000), Rain profiling algorithm for the TRMM Precipitation Radar, Journal of Applied Meteorology, 39 (12), pp. 2038-2052.
7. Jobard I., and M. Desbois (1994), Satellite estimation of the tropical precipitation using the Meteosat and SSM/I data, Atmospheric Research, 34, pp. 285–298.
8. Joyce R., J. E. Janowiak, and P. A. Arkin, P. Xie (2004), CMORPH: A Method that Produces Global Precipitation Estimates from Passive Microwave and Infrared Data at High Spatial and Temporal Resolution. Journal of Hydrometeorology, 5, pp. 487-503.
9. Mishra A., R M. Gairola, A K. Varma, Abhijit Sarkar and V. K Agarwal (2009), Rainfall Retrieval over Indian land and oceanic regions from SSM/I Microwave data, Advances in Space research, 44, pp. 815-823.
10. Mishra A., R M Gairola, A K Varma and V K Agarwal (2009), Study of Intense Heavy Rainfall Events over India Using KALPANA-IR and TRMM- Precipitation Radar Observations, Current Science, 9, 5, pp. 689-695.

11. Mishra A., R M Gairola, A K Varma and V. K. Agarwal, (2010), Remote sensing of Precipitation over Indian land and oceanic regions by synergistic use of multi-satellite sensors, Journal of Geophysical Research, 115, D08106, doi: 10.1029/2009JD012157.
12. Rahman, S. H. D. Sengupta, and M. Ravichandran (2009),Variability of Indian summer monsoon rainfall in daily data from gauge and satellite, Journal of Geophysical Research, 114, D17113, doi:10.1029/2008JD011694.
13. Roca, R., M. Viollier, L. Picon and M. Desbois (2002), A multisatellite analysis of deep convection and its moist environment over the Indian Ocean during the winter monsoon, Journal of Geophysical Research, 107, D19, 10.1029/2000JD000040.
14. T. Kubota, S. Shige, H. Hashizume, K. Aonashi, N. Takahashi, S. Seto, M. Hirose, Y. N. Takayabu, K. Nakagawa, K. Iwanami, T. Ushio, M. Kachi, and K. Okamoto, (2007) Global Precipitation Map using Satelliteborne Microwave Radiometers by the GSMaP Project, IEEE Transaction on Geoscience and Remote Sensing, 45, 7, pp.2259-2275.
15. Yatagai, A. O. Arakawa, K. Kamiguchi, H. Kawamoto, M. I. Nodzu and A. Hamada (2009), A 44-year daily gridded precipitation dataset for Asia based on a dense network of rain gauges, SOLA , 5, pp. 137-140, DOI:10.2151/sola.2009-035.